**Aalto University**

Chandra, Sourov; Sciortino, Alice; Shandilya, Shruti; Fang, Lincan; Chen, Xi; Nonappa; Jiang, Hua; Johansson, Leena Sisko; Cannas, Marco; Ruokolainen, Janne; Ras, Robin H.A.; Messina, Fabrizio; Peng, Bo; Ikkala, Olli

# Core-Selective Silver-Doping of Gold Nanoclusters by Surface-Bound Sulphates on Colloidal Templates: From Synthetic Mechanism to Relaxation Dynamics

# RESEARCH ARTICLE

# Core-Selective Silver-Doping of Gold Nanoclusters by Surface-Bound Sulphates on Colloidal Templates: From Synthetic Mechanism to Relaxation Dynamics

*Sourov Chandra,\* Alice Sciortino, Shruti Shandilya, Lincan Fang, Xi Chen,\* Nonappa, Hua Jiang, Leena-Sisko Johansson, Marco Cannas, Janne Ruokolainen, Robin H. A. Ras, Fabrizio Messina, Bo Peng,\* and Olli Ikkala*

**Ultra-small luminescent gold nanoclusters (AuNCs) have gained substantial interest owing to their low photobleaching and high biocompatibility. While the substitution of silver for gold at the central core of AuNCs has shown significant augmentation of photoluminescence with enhanced photostability, selective replacement of the central atom by silver is, however, energetically inhibited. Herein, a new strategy for in situ site-selective Ag-doping exclusively at the central core of AuNCs using sulphated colloidal surfaces as the templates is presented. This approach exceedingly improves the photoluminescence quantum efficiency of AuNCs by eliminating nonradiative losses in the multi-step relaxation cascade populating the emissive state. Density functional theory predicts the mechanism of specific doping at the central core, endorsing the preferential bonding between $Ag^+$ ions and sulphates in water. Finally, the generic nature of the templating concept to allow core-specific doping of nanoclusters is unraveled.**

## 1. Introduction

Luminescent nanomaterials (LNMs) are highly effective and versatile probes for optoelectronics, devices, catalysis, biomedical imaging, and theragnostic applications.[1–3] Various LNMs, including semiconductor quantum dots,[4] rare earth metal ions,[5] and silicon-based nanocrystals are well documented in the literature.[6] However, most of the existing water-borne LNMs are either highly cytotoxic or undergo photobleaching, limiting their application.[7,8] Therefore, there is a pressing need to develop water-borne LNMs with promoted photostability and biocompatibility. Recently, ultrasmall gold nanoclusters (AuNCs) have emerged as the state-of-the-art LNMs because of their remarkable optical properties, photostability, water dispersibility, and biocompatibility.[9–11] However, poor photoluminescence (PL) quantum yields (QYs) in comparison to quantum dots and organic dyes restrict their potential applications.[11] Doping the gold core is one of the significant approaches to increase their quantum efficiency.[12] Various techniques have been reported to optimize the metal compositions and the electronic structures of the subsequent nanoclusters (NCs).[13–15] Several metal atoms, including Pd, Pt, Ag, Cu, Hg, Ir, Cd, and Mn have been used as the dopant elements to selectively replace Au atoms in AuNCs.[13,15–18]

Ligand-protected AuNCs are usually composed of a metallic Au(0) core that is enclosed by Au(I)-thiolate oligomeric motifs, referred to "staples".[9] For instance, the $[Au_{25}(SR)_{18}]^-$ NC consists of an icosahedral core containing 13 atoms of Au(0) surrounded by the staples having six units of -S-Au-S-Au-S- motifs. The core can be further classified into two geometrical equivalencies: one central core atom surrounded by 12 equivalent outer core atoms. Therefore, there are three possible positions to incorporate the foreign elements: i) Central core, ii) outer core, and iii) staple motifs.[13] As a result, doping at the specific positions of an AuNC with a precise number of heteroatoms is still one of the most challenging tasks.[19,20] Density functional theory (DFT) calculations have shown that Ni, Pd, and Pt selectively replace the central core atom of the AuNCs. In contrast, Ag, Cd, Hg, and Mn prefer the substitution of the outer

S. Chandra, S. Shandilya, L. Fang, X. Chen, H. Jiang, J. Ruokolainen,
R. H. A. Ras, B. Peng, O. Ikkala
Department of Applied Physics
Aalto University
P. O. Box 15100, Espoo FI-00076, Finland
E-mail: sourov.chandra@aalto.fi; xi.6.chen@aalto.fi;
pengbo006@gmail.com, bo.peng@aalto.fi

A. Sciortino, M. Cannas, F. Messina
Dipartimento di Fisica e Chimica – Emilio Segrè
Università degli Studi di Palermo
Via Archirafi 36, Palermo 90123, Italy

A. Sciortino, M. Cannas, F. Messina
CHAB – ATeN Center
Università degli studi di Palermo
viale delle scienze, Edificio 18, Palermo 90128, Italy

Nonappa
Faculty of Engineering and Natural Sciences
Tampere University
P.O. Box 541, Tampere FI-33101, Finland

L.-S. Johansson
Department of Bioproducts and Biosystems
Aalto University
Vuorimiehentie 1, Espoo FI-00076, Finland

**ADVANCED**
**SCIENCE NEWS**
www.advancedsciencenews.com

**ADVANCED**
**OPTICAL**
**MATERIALS**
www.advopticalmat.de

core.[21,22] Wang et al. demonstrated that $Ag_xAu_{25-x}$ NCs with $x \leq$ 12 display nearly identical optical properties to undoped $Au_{25}$ NCs. The substitution takes place exclusively at the outer core and the NCs with $x = 1$ to 12 are weakly photoluminescent.[12] On the contrary, a huge increment of PL has been observed in $Ag_{13}Au_{12}$, due to the replacement of all 13 core atoms, including the central atom. $Ag_{13}Au_{12}$ NCs with $Ag_{13}$-core exhibit a relaxation dynamic remarkably faster than their undoped counterpart $Au_{25}$ NCs.[23] The central Ag atom could enhance the rigidity of $Ag_{13}Au_{12}$ NC by alleviating the charges in its lowest unoccupied molecular orbital (LUMO), leading to its strong luminescence.

Although the above results show that an Ag atom in the central core of AuNCs drastically influences their optical and electronic properties, there are no reports to date in which Ag-atom selectively replaces the Au atom at the central position without affecting other atoms in its outer core. All outer-core atoms need to be substituted one by one before reaching the central core.[12,24] It has been shown theoretically that the substitution at the central core is energetically unfavorable in contrast to other sites.[17,21] In addition, the highest relative energy along with the lowest HOMO-LUMO gap declines the Ag-doping in the central core.[21,22] While the substitution of high amount of Ag at the core of AuNCs exceedingly improves the quantum efficiency, the continuous leaching of $Ag^+$ ions makes the doped NCs highly cytotoxic. Moreover, photo-oxidation of the silver core diminishes its overall photostability.

Herein, we demonstrate a versatile one-pot synthetic strategy that allows in situ selective doping of Ag atoms at the central core of the AuNCs. Cellulose nanocrystals (CNCs) are selected as the model colloidal templates that are abundant in sulfate half-ester groups (-$OSO_3^-$) over surfaces,[25,26] promoting the growth of NCs with concurrent doping. The -$OSO_3^-$ groups could selectively anchor $Ag^+$ ions followed by the accumulations of various Au(III) complexes in water, leading to the formation of NCs with specific Ag-doping at the central core. DFT calculations clarify the prioritized anchor of $Ag^+$ ions by CNC-$OSO_3^-$ in water, suggesting a plausible formation mechanism of Ag-doping. Effectively, the doped NCs show a relaxation dynamic different from its subsequent undoped NCs and a strongly enhanced PL QY. An exceedingly small fraction of Ag in AuNCs assures their high biocompatibility. Moreover, their bright PL, polarizability, and high photostability make them unique among water-borne luminescent nanomaterials.
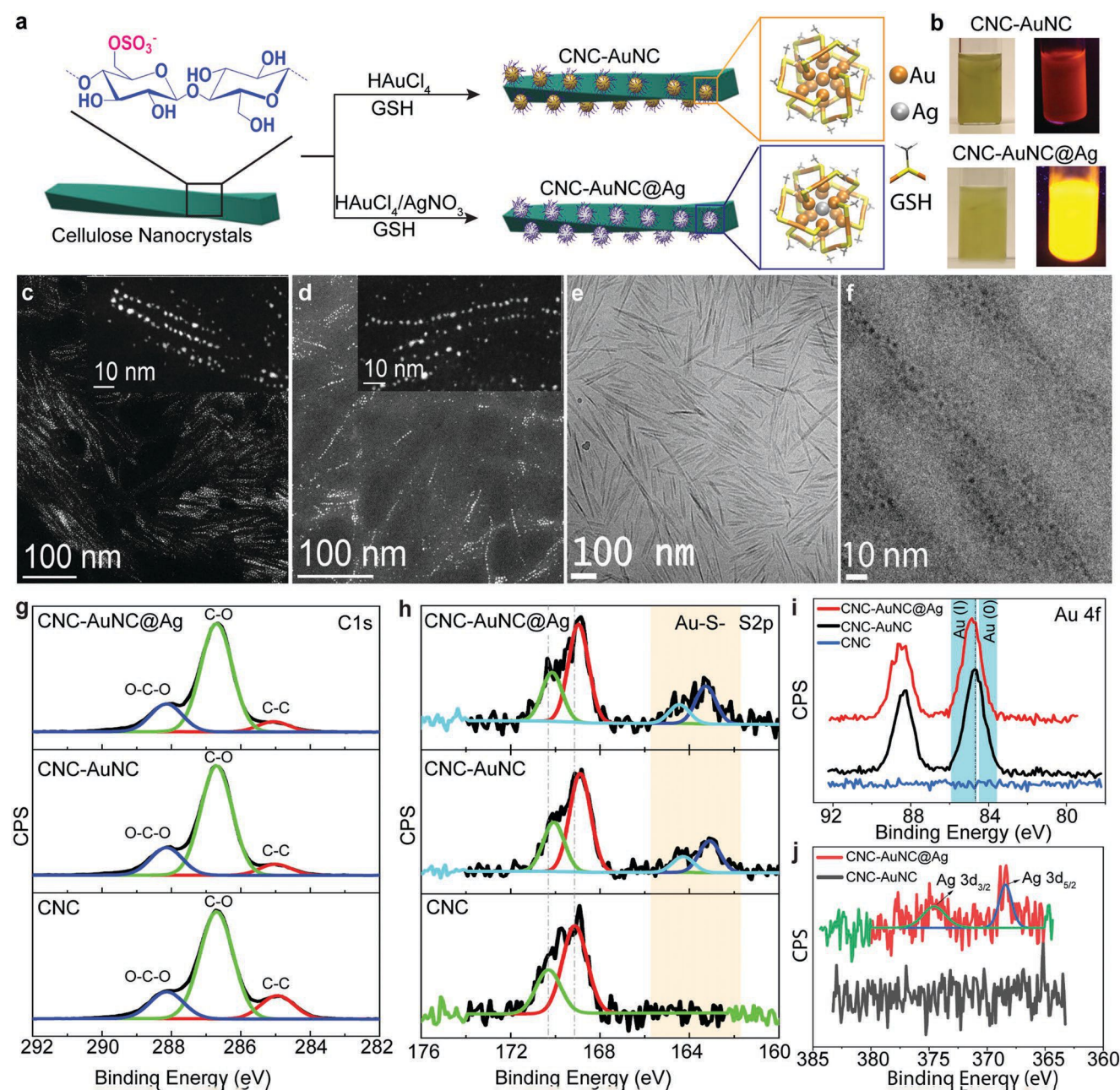
## 2. Results and Discussion

### 2.1. Synthesis and Characterizations

In this work, we have synthesized and studied i) AuNCs, ii) AuNCs decorated over sulphated (-$OSO_3^-$ groups) CNC surfaces, iii) Ag-doped AuNCs decorated over sulphated CNCs surfaces, and iv) control experiments using different colloidal particles and surface functionalities (-$COO^-$ and -$OPO_3^-$). In all experiments, glutathione has been used as the capping ligand for NCs. **Figure 1**a summarizes the components and methods used for the preparation of highly luminescent cellulose nanocrystals (CNCs) decorated with AuNCs (CNC-AuNCs) and Ag-doped AuNCs (CNC-AuNC@Ag). We used cotton-based

CNCs as the colloidal template because of their surface-rich sulfate-half ester (-$OSO_3^-$) groups (see Supporting Information for details).[27] The -$OSO_3^-$ groups over CNCs facilitate the formation and the synchronized site-specific Ag doping at the central core of AuNCs. The concentration of CNCs plays a crucial role in the formation and stability of NCs over the CNC surfaces (Figure S1, Supporting Information). Increasing the concentration of CNCs enhances the stability of NCs over their surfaces; the optimized concentration of CNC is 14.5 mg mL$^{-1}$. Figure 1b displays the aqueous dispersions of CNC-AuNC and CNC-AuNC@Ag under ambient light (upper panels) and exposure to UV-light (lower panels). It is evident that the emission from aqueous CNC-AuNC@Ag is substantially brighter than that of the corresponding CNC-AuNC. The transmission electron microscopy (TEM) image of CNCs (Figure S2a, Supporting Information) suggests their average length and width of 200 nm and 5 nm, respectively, which is well retained in CNC-AuNC@Ag nanocomposites (Figure S2b, Supporting Information). To compare with CNC-NCs composites, glutathione (GSH) capped AuNCs (i.e., without CNC template) have been synthesized according to a procedure described by Luo et al.[28] The AuNCs show a uniform particle distribution with an average size of 1.5 nm (Figure S2c, Supporting Information). The scanning transmission electron microscopy (STEM) images shown in Figure 1c,d reveal the uniform distribution of AuNCs and Ag-doped AuNCs, respectively, aligning linearly over the CNCs. Interestingly, the spacing between two consecutive NCs is around 5 nm, correlating with the distance between two adjacent -$OSO_3^-$ groups over CNC.[29] The cryo-TEM image (Figure 1f) also shows the inter-particle distances between 4.7 to 5 nm. Energy dispersive X-ray mapping of CNC-AuNC@Ag (Figure S3, Supporting Information) demonstrates the existence of Au, S, and C-rich phases. Finally, inductively coupled plasma optical emission spectrometry confirms the atomic ratio of Au : Ag = 15 : 1 with a mass content of 2.65% metals in CNC-AuNC@Ag. Thermogravimetric analysis (Figure S4, Supporting Information) reveals the existence of ≈2.6% of metals in CNC-AuNC@Ag.

To determine the surface functionalities and the binding interactions between CNC and NCs, X-ray photoelectron spectroscopy (XPS) has been performed (Figure S5, Supporting Information). The XPS spectra confirm the presence of C, O, N, and S atoms in CNC, and an additional Au peak in CNC-NCs. The C 1s XPS spectrum of the pristine CNCs shows three distinct peaks at 288.2, 286.7, and 284.9 eV, assign to O-C-O, -C-O, and C-C bonds, respectively (Figure 1g).[30] Therein, the spectral patterns of CNC-AuNC and CNC-AuNC@Ag are similar to that of the CNC itself. However, the higher ratio of oxygenated carbon species in CNC-AuNC and CNC-AuNC@Ag (O-C-O and -C-O groups) as compared to the C–C bonds is due to the presence of dicarboxylic acids in GSH ligands. The doublet S 2p3/2 and S 2p1/2 peaks at 169.1 and 170.3 eV, respectively, corresponds to the -$OSO_3^-$ groups in pristine CNC (Figure 1h). A small shift of around 0.2 eV in CNC-NC composites suggests a strong interaction of -$OSO_3^-$ with metals. An additional S 2p doublet at a lower oxidation state at 163.1 and 164.2 eV in both CNC-AuNC and CNC-AuNC@Ag indicates the presence of gold-thiolate bonds in the NCs.[25] As -$OSO_3^-Na^+$ turns out to be fully dissociated in water, the CNCs display a zeta potential

**ADVANCED
SCIENCE NEWS**

www.advancedsciencenews.com
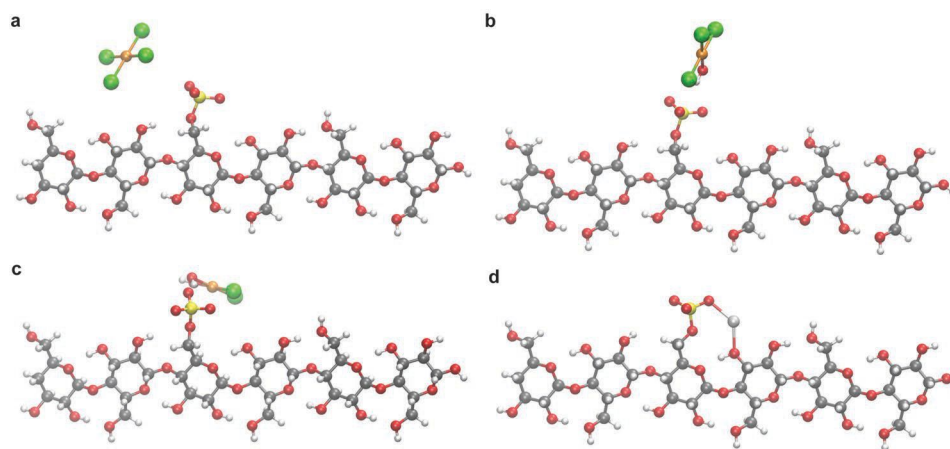
**ADVANCED
OPTICAL
MATERIALS**

www.advopticalmat.de

**Figure 1.** a) Schematic representation for the preparation AuNCs and AuNC@Ag over the surface of sulphated CNCs. b) As prepared CNC-AuNC and CNC-AuNC@Ag in water under ambient light (upper panel) and exposure of UV-light (lower panel). STEM images of c) CNC-AuNC and d) CNC-AuNC@Ag (Insets in c) and d) are the corresponding high-resolution images). e) and f) Cryo-TEM images of CNC-AuNC@Ag. g) C 1s, h) S 2p, i) Au 4f and j) Ag 3d XPS spectra of CNC, CNC-AuNC, and CNC-AuNC@Ag.

value of −70 mV at pH 7. However, the potential values are slightly lower in both CNC-AuNC (−59 mV) and CNC-AuNC@Ag (−53 mV) which further confirms the strong bonding among the -OSO$_3^-$ groups in CNC and the metal atoms of the NCs. The presence of Au atoms and their Au(0) valence state along with Au(I) binding motifs in both CNC-AuNC and CNC-AuNC@Ag are evidenced by Au 4f XPS spectrum (Figure 1i).[31] However, a small shift in Au 4f binding energy (0.2 eV) might be associated to large charge redistribution in Au−Au coupling caused by Ag-doping.[16] A trace amount of Ag atom has been

detected (Figure 1j) in CNC-AuNC@Ag, cluing the Ag-doping likely at the interior of AuNCs.

## 2.2. DFT Exploration of Formation Mechanism

To gain insight on the position of Ag atoms in CNC-AuNC@Ag and to explore the origin of optical enhancement, we performed DFT calculations. In DFT, the well-defined [Au$_{25}$(SR)$_{18}$]$^{-1}$ NCs have been used as a model cluster. Glutathione (ligand) is

**ADVANCED**
**SCIENCE NEWS**

www.advancedsciencenews.com

**ADVANCED**
**OPTICAL**
**MATERIALS**

www.advopticalmat.de

**Figure 2.** The optimized structures of CNC-OSO$_3^-$ in association with a) AuCl$_4^-$, b) [AuCl$_3$(OH)]$^-$, c) [AuCl$_2$(OH)$_2$]$^-$, and d) Ag$^+$.

replaced by -SCH$_3$ to simplify the computational complexity. The reasons behind the selection of Au$_{25}$ as the model cluster are the adjoining number of atoms (Au$_{29}$-Au$_{43}$) in AuNCs that we have reproduced here in accordance with Luo et al.,[28] along with their similar optical properties. Moreover, [Au$_{25}$(SR)$_{18}$]$^{-1}$ NCs have been extensively studied in this size regime[32] and therefore its atomic coordinates are well recognized. We have simulated three possible structures of [Ag$_1$Au$_{24}$(SR)$_{18}$]$^{-1}$ NCs (Figure S6, Supporting Information) by mono-metal doping at the central core (Au$_{24}$@Ag$_{cn}$), outer core (Au$_{24}$@Ag$_{oc}$), and at the staple motif (Au$_{24}$@Ag$_{sm}$) of the NCs. Furthermore, we have also simulated two possible structures of [Ag$_2$Au$_{23}$(SR)$_{18}$]$^{-1}$, in which one Ag atom is at the center and the other is either in the outer core (Au$_{23}$@Ag$_{cn+oc}$) or in the staple motif (Au$_{23}$@Ag$_{cn+sm}$). All clusters have been optimized by the DFT method (see Methods for details, Supporting Information). The relative energy and the HOMO-LUMO energy gap of the NCs are presented in Table S1, Supporting Information and their atomic projected density of states are shown in Figure S7, Supporting Information. Amongst [Ag$_1$Au$_{24}$(SR)$_{18}$]$^{-1}$ NCs, Au$_{24}$@Ag$_{cn}$ with an Ag atom at the central core is energetically unfavorable owing to the highest relative energy in comparison to its other positional isomers (Au$_{24}$@Ag$_{oc}$ and Au$_{24}$@Ag$_{sm}$).[17,21] Both Au$_{24}$@Ag$_{oc}$ and Au$_{24}$@Ag$_{sm}$ consist of very similar HOMO-LUMO gap to that of their parent Au$_{25}$ entity (1.253 eV). The Ag atom in these two clusters offers a negligible contribution to the electronic state of Au$_{25}$ near the Fermi levels that determine the optical properties of the NCs. So, one could expect their optical behavior analogous to the Au$_{25}$ NCs. In contrast, Au$_{24}$@Ag$_{cn}$ has a reduced bandgap of 1.099 eV in which the HOMO states are significantly contributed by the Ag orbitals. As a result, its optical properties should be different than that of its parent Au$_{25}$ NCs. Furthermore, the Ag atom in Au$_{23}$@Ag$_{cn+oc}$ and Au$_{23}$@Ag$_{cn+sm}$ has slightly more contribution to the electronic states near the Fermi level than that of the Au$_{24}$@Ag$_{cn}$, having HOMO-LUMO energy gap of 1.052 and 1.045 eV, respectively. These observations signify the unique importance for the site-specific central core doping of Ag in AuNCs.

Next, we would like to explore the probable mechanism of Ag-doping at the core of the AuNCs in presence of CNCs. In

aqueous medium, AgNO$_3$ immediately dissociates into Ag$^+$ and NO$_3^-$ ions. In contrast, HAuCl$_4$ derives four coordinate square planar complexes in water:[33,34] [AuCl$_x$(OH)$_{4-x}$]$^-$ ($x >$ 2) at pH < 7 along with free Cl$^-$ ions.[35,36] The free Cl$^-$ ions induce the immediate precipitation of insoluble AgCl upon mixing of AgNO$_3$ and HAuCl$_4$ in water (Figure S8, Supporting Information). Surprisingly, the addition of CNCs has overruled this sedimentation, indicating the absence of free Ag$^+$ ions in this system. Therefore, in our experiment, Ag$^+$, AuCl$_4^-$, and [AuCl$_3$(OH)]$^-$ are subsidizing as the major ions in addition to a minor amount of [AuCl$_2$(OH)$_2$]$^-$ ions in the solution.

To study the mechanism of how the ions could interact with CNC-OSO$_3^-$, we have calculated their bonding energies in water.[37] The geometry of CNC-OSO$_3^-$ has been built up based on the atomic structures reported elsewhere.[38] We use the finite unit as shown in **Figure 2** for the simulations, in which H atoms are saturated at the left and right ends of the complexes. After optimizing the CNC-OSO$_3^-$, we introduce Ag$^+$, AuCl$_4^-$, [AuCl$_3$(OH)]$^-$, and [AuCl$_2$(OH)$_2$]$^-$ individually near the -OSO$_3^-$ group of the substrate with four different initial positions. After the energy of the relaxed structures converged, the one with an energy minimal has been used to calculate the bonding energy. The optimized structures are shown in Figure 2. All Au(III) ions including AuCl$_4^-$, [AuCl$_3$(OH)]$^-$ and [AuCl$_2$(OH)$_2$]$^-$ exhibit positive bonding energies to CNC-OSO$_3^-$ in water with bonding energies 0.127, 0.182 and 0.091 eV, respectively. Hence, they would not form stable complexes with CNC-OSO$_3^-$. On the contrary, Ag$^+$ could easily facilitate a strong bond with the -OSO$_3^-$ groups owing to the negative bonding energy of −0.997 eV in water. Although Au$^+$ ion enables to form the most stable bond with CNC-OSO$_3^-$ (bonding energy −1.662 eV, Figure S9, Supporting Information), the probability for the formation of Au(I) by the reduction of Au(III)-chloride complexes in water without GSH will be nil. The results conclude that sulphated CNCs enable the formation of CNC-OSO$_3^-$ Ag$^+$ at first, followed by Ag$_x$Au$_y$ alloy clusters in accumulation of Au(III) complexes or Au$^+$ ions upon reduction, in which Ag places at the center of the NCs.

## 2.3. Optical Properties

The aqueous dispersions of CNC-AuNC and CNC-AuNC@Ag exhibit a similar featureless steady-state absorption spectrum at 400 nm (**Figure 3**a), to that of individual AuNCs (Figure S10, Supporting Information).[28] However, upon templating the NCs over CNCs, the composites exhibit an attenuated optical absorption in compared to the bare AuNCs. This is attributed to
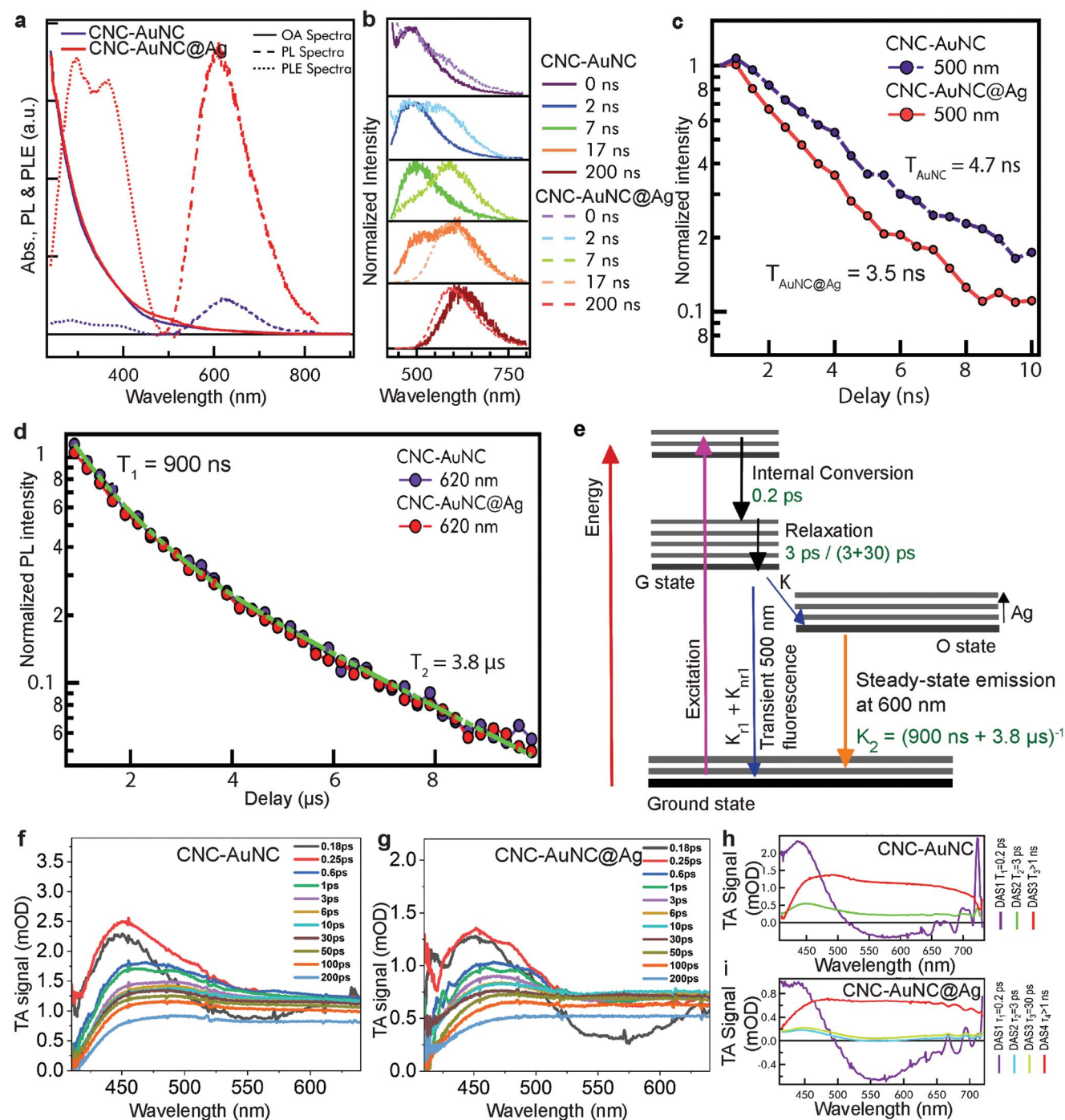


**Figure 3.** a) Steady-state optical property of the aqueous dispersions of CNC-AuNC (purple) and CNC-AuNC@Ag (red): UV-vis absorption spectra (continuous curves), PL emission spectra excited at 410 nm (dashed curves), and photoluminescence excitation (PLE) spectra at 600 nm emission (dotted curves). b) Comparison of emission spectrum between CNC-AuNC (continuous curves) and CNC-AuNC@Ag (dashed curves) recorded at different time delays (indicated in the legend) from photoexcitation. Spectra delayed at 0 to 7 ns and 17 to 200 ns were acquired within a gate window of 0.5 and 10 ns from the indicated delay, respectively. PL kinetic traces recorded at c) 500 nm and d) 600 nm, upon 410 nm excitation. e) Model describing the relaxation of photoexcited CNC-AuNC and CNC-AuNC@Ag. TA spectra excited at 400 nm, as measured in a solution of f) CNC-AuNC and g) CNC-AuNC@Ag at different delays after the photoexcitation. DAS of h) CNC-AuNC and (i) CNC-AuNC@Ag with the respective lifetimes.

**ADVANCED
SCIENCE NEWS**

www.advancedsciencenews.com

**ADVANCED
OPTICAL
MATERIALS**

www.advopticalmat.de

the high content of CNCs with respect to the NCs (≈2.6%) along with their overlapping absorptions.[25] The AuNCs prepared in the presence and absence of CNCs show nearly identical optical properties (Figure S10, Supporting Information). This suggests that they are identical with each other and AuNCs retained their intrinsic optical properties after conjugation over the CNCs.[25] Notably, Ag-doping significantly promotes the PL emission in contrast to the undoped CNC-AuNC or the individual AuNCs. The absolute QY of CNC-AuNC@Ag is ≈23%, around 6.5 times higher than that of the CNC-AuNC (3.5%). In addition, the circular dichroism spectrum (Figure S11, Supporting Information) of CNC-AuNC is similar to that of individual AuNCs. The peaks are centered at ∼ 360 nm, indicating that the CNCs would not affect the structure of grafted NCs. However, the spectrum of CNC-AuNC@Ag exhibits a redshift with a peak maximum at ≈374 nm along with a decreasing value of ellipticity.[39] Such a redshift of ≈14 nm can be explained by DFT calculations. We have observed that the substitution of Au by Ag at the central core of the AuNCs significantly reduces the HOMO-LUMO gap that causes a red shift of the time-dependent density functional theory-computed absorption spectra (Figure S12, Supporting Information). On contrary, doping an Ag atom at other sites have negligible effects on the HOMO states and hence on their optical absorption spectra. The results further support the unique impact of the site-selective doping of Ag.

To investigate the origin of this significant increment of PL emission, the relaxation dynamics of excited-state carriers of CNC-AuNC and CNC-AuNC@Ag have been studied using nanosecond and femtosecond time-resolved measurements upon excitation with a pulsed laser. These data reveal that the orange-emitting state is populated through an intermediate, and the different QYs of the two samples arise from different efficiencies of this intermediate population step. In fact, immediately after photoexcitation at 410 nm, CNC-AuNC displays an emission peak at 500 nm (Figure 3b – upper panel), decaying with a lifetime of 4.7 ns (Figure 3c). This emission is only transient and hence negligibly contributes to the steady-state emission. Within a few nanoseconds, it rapidly gives way to long-lived emission peaking at 620 nm. The latter band appears with a delayed onset of several nanoseconds (Figure 3b), and then displays a bi-exponential decay with lifetimes of $T_1 = 900$ ns and $T_2 = 3.8$ µs (Figure 3d). These data suggest the involvement of two excited states (Figure 3e): the former one (state G) is depopulated very quickly, producing an emission in the green region, and simultaneously feeding the second state O; the latter one, after its population, is responsible of the foremost orange emission with long lifetimes ($K_2$). The two processes, depopulation of state G and population of state O, compete during similar time scales, and probably the former is more efficient than the latter considering the low QY of orange emission in CNC-AuNC. Depopulation of G towards ground-state ($K_{r1}+K_{nr1}$) is fast and prevalently non-radiative, so that the steady-state green emission is negligible. The same experiments have also been performed on the aqueous dispersion of CNC-AuNC@Ag. However, the orange band appears much earlier than in the CNC-AuNCs, indicating more efficient population of the O state from G. So, the addition of silver atom at the central core of AuNCs strongly enhances the population channel (K) of O competing with depopulation of the G state, defining shorter lifetime (3.5 ns instead of 4.7 ns) in 500 nm emission decays.

Additionally, we have performed the pump-probe measurements to investigate the dynamics in the sub-ns temporal range. As shown in Figures 3f,g, the transient absorption (TA) signal is broad, unstructured, and undergoes relaxation in a time range of a few picoseconds. No significant decay of the overall intensity is visible in this time range, indicating negligible population losses within the first ns. Furthermore, the singular value decomposition global analysis could quantify the time scales and define the associated spectral evolution. The TA dynamics of the CNC-AuNC signal can be described by three timescales: $\tau_1 = 0.2$ ps, $\tau_2 = 3$ ps, and $\tau_3 > 1$ ns, and the three decay-associated spectra (DAS) are shown in Figure 3h. From the shape of the DAS it can be inferred that the fastest process ($\tau_1$) leads to a substantial change of the TA signal shape with a decay of a positive excited-state absorption component at ≈450 nm and the growth of a broad and redshifted excited-state absorption in 520–650 nm region. Such a substantial change of the optical fingerprint of the electronic state is most likely due to an internal conversion from the initially excited state $S_n$ down to the nanosecond-emissive manifold (i.e., state G in Figure 3c) from which the nanosecond dynamics further proceeds at longer times.[40,41] The DAS associated to the second relaxation component ($\tau_2$) leads to minor spectral changes of the TA signal in the picosecond range, spreading over the whole wavelength region of the probe. These changes can be attributed to structural stabilization and thermalization within the emissive manifold.[40,42] However, the same analysis on the CNC-AuNC@Ag (Figure 3i) highlights the appearance of a new temporal component of $\tau = 30$ ps. Thus, the Ag-doping is responsible for the overall slowing down of the relaxation from 3 ps (single-exponential) to 3 ps + 30 ps (bi-exponential). The Ag-doping, therefore, leads to a more pronounced and longer excited-state relaxation than the undoped one, which is indeed consistent with the observed PL shifts.
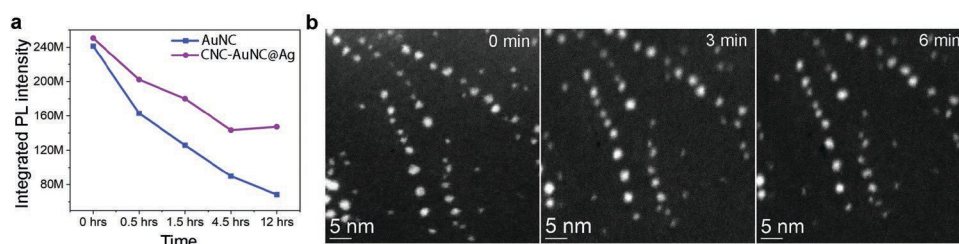
Individual AuNCs are unstable and tend to agglomerate when exposed to UV light or electron beam, resulting in plasmonic gold nanoparticles.[43] However, the photostability of the NCs, templated by CNCs, has significantly improved. This is due to the high restrictions on the movement of the NCs by their strong bonding with CNCs. Indeed, CNC-AuNC@Ag remains photostable under continuous UV irradiation for 12 h (**Figure 4**a). Even under the exposure of electron beams up to 6 min, no substantial transformation of particle size has been identified (Figure 4b).

In addition, the collective optical properties of CNC-NCs films have been studied using polarized optical microscopy (Figure S13, Supporting Information). The optical birefringence[44] caused by assembled chiral nematic structures of the CNC-AuNC@Ag become pronounced in contrast to CNCs. This is probably due to the synchronized effects of strong PL from AuNC@Ag and robust polarization by well-defined chiral nematic phase of CNC building blocks (Figure S14, Supporting Information).[45]

## 2.4. Bonding Affinity of Ag⁺ and Au (III) Complex Ions to Different Surface Functional CNCs

To compare the effect of different surface functionalities in Ag-doping, CNCs with $-PO_4^{2-}$, -COOH, and -OH groups are

**ADVANCED
SCIENCE NEWS**

www.advancedsciencenews.com

**ADVANCED
OPTICAL
MATERIALS**

www.advopticalmat.de

**Figure 4.** a) Photostability of CNC-AuNC@Ag and individual AuNCs under exposure of UV-light. b) Stability of CNC-AuNC@Ag under the continuous exposure of electron beam for 0, 3, and 6 min.

simulated upon interactions with $Ag^+$, $AuCl_4^-$, $[AuCl_3(OH)]^-$, and $[AuCl_2(OH)_2]^-$ ions in water. Figures S15–S17, Supporting Information show the optimized structures of CNC-OPO$_3^{2-}$, CNC-COO$^-$, and CNC-O$^-$ in association with ions, and their bonding energies are enlisted in Table S2, Supporting Information. It is noteworthy to mention that only CNC-OSO$_3^-$ among all others shows positive bonding energies to the Au(III) ions and complexes along with strong negative bonding energy to $Ag^+$. In addition, its strongly negative potential of −70 mV at pH 7 prefers an immediate bonding with $Ag^+$, followed by Au(III) or $Au^+$ ions, directing the in situ Ag-doping at the central-core of the AuNCs. On the contrary, CNC-OPO$_3^{2-}$ displays preferable (negative) bonding with both $Ag^+$ and Au(III) complexes in water. Although CNC-OPO$_3^{2-}$ $Ag^+$ is the most stable form, the concentration of Au(III) ions or complexes would be much higher than that of the $Ag^+$ ions. As a result, there would be a strong contest in between $Ag^+$ and Au(III) ions, thus interrupting the specific and selective doping at the central core. In our experiment, the growth of AuNC or AuNC@Ag over the CNC-OPO$_3^{2-}$ surface have been completely abortive, probably due to the very lower amount of surface phosphate groups and hence their low zeta-potential (-11 mV) in water at pH 7. Similarly, CNC-COO$^-$ shows negative bonding energies with all of the ions including $AuCl_4^-$. Moreover, its low ionization potential

at pH < 7 due to poor conversation of –COOH to –COO$^-$ at neutral or acidic conditions would make them even incompetent to form NCs over CNCs. The dissociation of CNC-OH to CNC-O$^-$ is negligible and hence could not be substantial for further interactions.

## 2.5. Generic Ag-Doping Over Sulphated Colloidal Templates

To investigate the role of -O-SO$_3^-$ groups responsible for the formation of AuNCs with their in situ core-specific Ag doping, we have further introduced sulphated polystyrene colloids as a generic template. The ample -OSO$_3^-$ groups over polystyrene particles have been identified by the Fourier-transform infrared spectroscopy (Figure S18, Supporting Information).[46] Similar to CNC-OSO$_3^-$, **Figure 5** reveals the successful deposition of AuNCs and Ag-doped AuNCs over the surface of polystyrene particles, as its insets show luminescence and enhanced luminescence. This is further verified by the TEM observation and elemental mapping. In addition, we have introduced -COOH groups to the polystyrene particles, which is again unsuccessful for the growth of AuNCs over their surfaces and synchronized Ag-doping (Figure S19, Supporting Information), experimentally verifying our speculation.
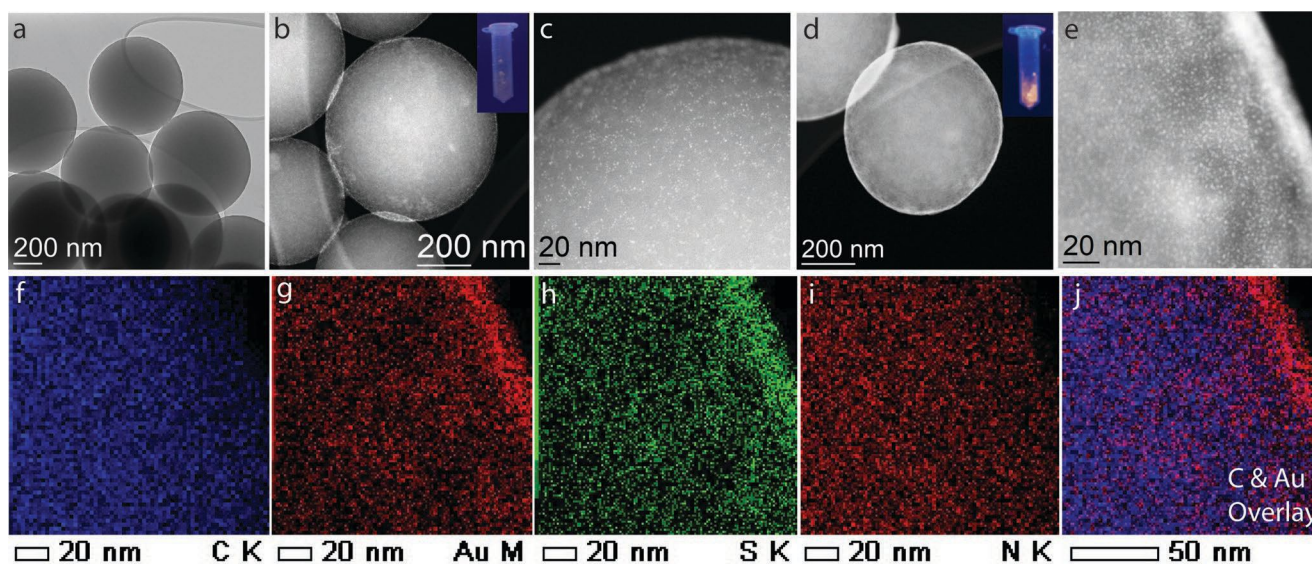


**Figure 5.** a) TEM image of sulphated polystyrene particles. STEM images of b,c) polystyrene-AuNC composite and d,e) polystyrene-AuNC@Ag composite. f–j) Energy dispersive X-ray mapping of polystyrene-AuNC@Ag.

**ADVANCED
SCIENCE NEWS**

www.advancedsciencenews.com

**ADVANCED
OPTICAL
MATERIALS**

www.advopticalmat.de

### 2.6. In Vitro Cytotoxicity

Finally, we evaluate the cytotoxicity of the CNC-AuNC@Ag against Human Dermal Fibroblasts (HDF). In the concentration range of 1–350 µM, the particles did not show apparent cytotoxicity to cells using MTT assay over 24 h (Figure S20, Supporting Information). Furthermore, we assess the reactive oxygen species generation (ROS) upon the uptake of CNC-AuNC@Ag in HDF using DCFH-DA assay-specific probe (Figure S21, Supporting Information). It shows no significant impact on intracellular ROS production compared to the control cells. Overall, these results unravel the non-toxic and non-reactive nature of CNC-AuNC@Ag in cells.

## 3. Conclusion

In conclusion, we have developed a new strategy for the templated synthesis of highly luminescent Ag-doped AuNCs on sulphated colloidal substrates, where the surface-bound -O-SO$_3^-$ groups lead to a site-specific Ag-doping at the central core of the AuNCs and make them robustly stable. The site-precise Ag-doping in AuNCs dramatically increases their PL quantum efficiency with superb photostability. This process has been verified theoretically and experimentally. CNC matrices further impose a robust polarization effect on CNC-AuNC@Ag composites due to their cholesteric orientation in dry state. The correlation of intense luminescence and optical polarization coupled with high biocompatibility may explore their future applications in optoelectronics, photocatalysis, and biomedicines. Even more generally, we foresee that different colloidal templates with -O-SO$_3^-$ surface groups can allow further tunable adducts, tunable for, e.g., biomedical applications.

## 4. Experimental Section

Detailed experimental materials and methods can be found in the Supporting Information.

## Supporting Information

Supporting Information is available from the Wiley Online Library or from the author.

## Acknowledgements

## Conflict of Interest

The authors declare no conflict of interest.

## Data Availability Statement

The data that support the findings of this study are available from the corresponding author upon reasonable request.

## Keywords

[1] F. Wang, W. B. Tan, Y. Zhang, X. Fan, M. Wang, *Nanotechnology* **2006**, *17*, R1.
[2] X. Zhu, Q. Su, W. Feng, F. Li, *Chem. Soc. Rev.* **2017**, *46*, 1025.
[3] J. Zhou, Q. Liu, W. Feng, Y. Sun, F. Li, *Chem. Rev.* **2015**, *115*, 395.
[4] D. Bera, L. Qian, T. K. Tseng, P. H. Holloway, *Materials* **2010**, *3*, 2260.
[5] B. Shao, J. Huo, H. You, *Adv. Opt. Mater.* **2019**, *7*, 1900319.
[6] S. Chandra, Y. Masuda, N. Shirahata, F. M. Winnik, *Angew. Chem., Int. Ed.* **2017**, *56*, 6157.
[7] F. M. Winnik, D. Maysinger, *Acc. Chem. Res.* **2013**, *46*, 672.
[8] M. Montalti, A. Cantelli, G. Battistelli, *Chem. Soc. Rev.* **2015**, *44*, 4853.
[9] R. Jin, C. Zeng, M. Zhou, Y. Chen, *Chem. Rev.* **2016**, *116*, 10346.
[10] S. Chandra, Nonappa, G. B. , A. Som, S. Zhou, J. Lahtinen, H. Jiang, J. V. I. Timonen, O. Ikkala, R. H. A. Ras, *Adv. Opt. Mater.* **2019**, *7*, 1900620.
[11] I. Chakraborty, T. Pradeep, *Chem. Rev.* **2017**, *117*, 8208.
[12] S. Wang, X. Meng, A. Das, T. Li, Y. Song, T. Cao, X. Zhu, M. Zhu, R. Jin, *Angew. Chem., Int. Ed.* **2014**, *53*, 2376.
[13] W. Fei, S. Antonello, T. Dainese, A. Dolmella, M. Lahtinen, K. Rissanen, A. Venzo, F. Maran, *J. Am. Chem. Soc.* **2019**, *141*, 16033.
[14] D. K. Pattadar, R. A. Masitas, C. D. Stachurski, D. E. Cliffel, F. P. Zamborini, *J. Am. Chem. Soc.* **2020**, *142*, 19268.
[15] S. Wang, Y. Song, S. Jin, X. Liu, J. Zhang, Y. Pei, X. Meng, M. Chen, P. Li, M. Zhu, *J. Am. Chem. Soc.* **2015**, *137*, 4018.
[16] E. Oh, J. B. Delehanty, L. D. Field, A. J. Mäkinen, R. Goswami, A. L. Huston, I. L. Medintz, *Chem. Mater.* **2016**, *28*, 8676.
[17] E. B. Guidez, V. Mäkinen, H. Häkkinen, C. M. Aikens, *J. Phys. Chem. C* **2012**, *116*, 20617.
[18] Y. Negishi, K. Munakata, W. Ohgake, K. Nobusada, *J. Phys. Chem. Lett.* **2012**, *3*, 2209.
[19] S. Wang, Q. Li, X. Kang, M. Zhu, *Acc. Chem. Res.* **2018**, *51*, 2784.
[20] S. Hossain, Y. Niihori, L. V. Nair, B. Kumar, W. Kurashige, Y. Negishi, *Acc. Chem. Res.* **2018**, *51*, 3114.
[21] F. Alkan, P. Pandeya, C. M. Aikens, *J. Phys. Chem. C* **2019**, *123*, 9516.
[22] M. G. Taylor, G. Mpourmpakis, *J. Phys. Chem. Lett.* **2018**, *9*, 6773.
[23] M. Zhou, J. Zhong, S. Wang, Q. Guo, M. Zhu, Y. Pei, A. Xia, *J. Phys. Chem. C* **2015**, *119*, 18790.
[24] A. Ghosh, O. F. Mohammed, O. M. Bakr, *Acc. Chem. Res.* **2018**, *51*, 3094.
[25] V. Hynninen, S. Chandra, S. Das, M. Amini, Y. Dai, S. Lepikko, P. Mohammadi, S. Hietala, R. H. A. Ras, Z. Sun, O. Ikkala, Nonappa, *Small* **2021**, *17*, 2005205.
[26] J. Majoinen, J. Hassinen, J. S. Haataja, H. T. Rekola, E. Kontturi, M. A. Kostiainen, R. H. A. Ras, P. Törmä, O. Ikkala, *Adv. Mater.* **2016**, *28*, 5262.
[27] V. Hynninen, S. Hietala, J. R. McKee, L. Murtomäki, O. J. Rojas, O. Ikkala, Nonappa, *Biomacromolecules* **2018**, *19*, 2795.

**ADVANCED
SCIENCE NEWS**

www.advancedsciencenews.com

**ADVANCED
OPTICAL
MATERIALS**

www.advopticalmat.de

[28] Z. Luo, X. Yuan, Y. Yu, Q. Zhang, D. T. Leong, J. Y. Lee, J. Xie, *J. Am. Chem. Soc.* **2012**, *134*, 16662.

[29] W. P. F. Neto, Morphological Investigation of Cellulose Nanocrystals and Nanocomposite Applications, Doctoral dissertation, Federal University of Uberlandia, **2017**.

[30] C. D. Edgar, D. G. Gray, *Cellulose* **2003**, *10*, 299.

[31] Y. Yang, A. Han, R. Li, G. Fang, J. Liu, S. Wang, *Analyst* **2017**, *142*, 4486.

[32] Y. Han, D. S. He, Y. Liu, S. Xie, T. Tsukuda, Z. Y. Li, *Small* **2012**, *8*, 2361.

[33] F. Farges, J. A. Sharps, G. E. Brown Jr., *Geochim. Cosmochim. Acta* **1993**, *57*, 1243.

[34] A. Usher, D. C. McPhail, J. Brugger, *Geochim. Cosmochim. Acta* **2009**, *73*, 3359.

[35] S. Wang, K. Qian, X. Bi, W. Huang, *J. Phys. Chem. C* **2009**, *113*, 6505.

[36] P. J. Murphy, M. S. LaGrange, *Geochim. Cosmochim. Acta* **1998**, *62*, 3515.

[37] A. Held, M. Walter, *J. Chem. Phys.* **2014**, *141*, 174108.

[38] U. Sternberg, F. T. Koch, W. Prieß, R. Witter, *Cellulose* **2003**, *10*, 189.

[39] S. Basu, M. P. Bakulić, H. Fakhouri, I. Russier-Antoine, C. Moulin, P. F. Brevet, V. Bonačić-Koutecký, R. Antoine, *J. Phys. Chem. C* **2020**, *124*, 19368.

[40] K. Pyo, V. D. Thanthirige, K. Kwak, P. Pandurangan, G. Ramakrishna, D. Lee, *J. Am. Chem. Soc.* **2015**, *137*, 8244.

[41] M. Zhou, C. Zeng, M. Y. Sfeir, M. Cotlet, K. Iida, K. Nobusada, R. Jin, *J. Phys. Chem. Lett.* **2017**, *8*, 4023.

[42] M. Zhou, C. Zeng, Q. Li, T. Higaki, R. Jin, *Nanomaterials* **2019**, *9*, 922.

[43] B. Weng, K. Q. Lu, Z. Tang, H. M. Chen, Y. J. Xu, *Nat. Commun.* **2018**, *9*, 1543.

[44] R. M. Parker, G. Guidetti, C. A. Williams, T. Zhao, A. Narkevicius, S. Vignolini, B. Frka-Petesic, *Adv. Mater.* **2018**, *30*, 1704477.

[45] K. Heise, E. Kontturi, Y. Allahverdiyeva, T. Tammelin, M. B. Linder, Nonappa, O. Ikkala, *Adv. Mater.* **2021**, *33*, 2004349.

[46] Y. Cong, T. Xia, M. Zou, Z. Li, B. Peng, D. Guo, Z. Deng, *J. Mater. Chem. B* **2014**, *2*, 3450.